PRINT ISSN 1119-8362
Electronic ISSN 1119-8362

Full-text Available Online at
https://www.ajol.info/index.php/jasem
https://www.bioline.org.br/ja

J. Appl. Sci. Environ. Manage.
Vol. 26 (2) 281-286 February 2022

Synthesis of Iron Oxide Magnetic Nanoparticles: Characterization and its Biomedical Application

USHA,V; AMUTHA, E; PUSHPALAKSMI, E; JENSON SAMRAJ, J; RAJADURAIPANDIAN, S; GANDHIMATHI, S; *ANNADURAI, G

*[*1]Division of Nano-science, Sri Paramakalyani Centre for Excellence in Environmental Sciences, Manonmaniam Sundaranar University, Alwarkurichi - 627 412, India*

[2]Sri Paramakalyani College, Department of Chemistry, Alwarkurichi - 627412, India
**Corresponding Author Email: gannadurai@msuniv.ac.in*

ABSTRACT: In the present time, Iron oxide magnetic nanoparticles (IOMNPs) have paid considerable attention due to their exclusive applications in terms of surface-to-volume ratio, superparamagnetism, high surface area, biosensor, bio-separation, catalysis, and biomedicine. Our goal was to synthesis iron oxide magnetic nanoparticles by chemical route technique. The preparation method had a very large effect on the size, shape, and surface chemistry of the magnetic nanoparticles including their applications. The iron chloride solution was prepared by mixing deionized water with iron chloride tetrahydrate. The synthesized powder was characterized by XRD, UV-vis, SEM, FT-IR, DLS, FL, and TGA techniques. Moreover, antibacterial activity was evaluated using the synthesized IOMNPs against *Escherichia coli* (A), *Pseudomonas* (B), *Enterobacter* (C), *Staphylococcus aureus* (D), and *Bacillus subtilis* (E) in the concentration of 0.1 mg and 0.5 mg. The results showed that *Bacillus subtilis* possess a higher antibacterial activity at the concentration of 0.5 mg comparing the other bacterial species. The outcome of this work would contribute to the present understanding of the biomedical application with the obtained size, shape, and synthesized method.

DOI: https://dx.doi.org/10.4314/jasem.v26i2.16

Impact factor: http://sjifactor.com/passport.php?id=21082

Google Analytics: https://www.ajol.info/stats/bdf07303d34706088ffffbc8a92c9c1491b12470

Keywords: IOMNPs, high surface area, iron chloride, SEM, and biomedical properties

Nanoscale materials are compatible with biomedical devices as most of the biosystems are nanosized. Inorganic, carbon nanotubes, metallic surfaces, and liposomes form the nanotechnology products that are used mostly in biomedical devices (Liu *et al.*, 2016). Metal oxide nanoparticles are hired to produce various biomedical devices in immunotherapy, tissue therapy, dentistry, wound healing, diagnosis, biosensing platforms, and regenerative medicines (Nikolova and Chavali, 2020). Iron oxide NPs have physical, optical, and magnetic properties (Mazrouaa *et al.*, 2019; Dadashi *et al.*, 2015). The magnetic properties present in the nanoparticle were best suitable for the magnetic separation of bioproducts and assists in site-specific drug delivery (Estelrich *et al.*, 2015). Iron oxide NPs in the therapeutic application is concentrated by the external magnetic field and are removed once the therapy is done. However, in bloodstreams, Iron oxide NPs are exposed to opsonization followed by recognition and exclusion (Roy *et al.*, 2014). In general, Iron oxide NPs are accepted to destroy cancer cells without negotiating the normal cells. This could be achieved with the magnetic nanoparticle by alternating the magnetic field, hysteresis heating, and frictional approach (Giustini *et al.*, 2010). Shi *et al.*, (2012) demonstrated the natural biopolymer chitosan-coated with iron oxide NPs to develop drug delivery against low bone mineral density like osteoporosis. (Arsalani *et al.*, 2020) reported the synthesis of iron oxide NPs using the thermal decomposition method for biomedical applications with both fluorescent and radioluminescent properties. Surface modification of iron oxide NPs proved to be more advantageous for different biomedical applications including cancer drug targeting and magnetic resonance imaging (MRI) (Dadfar *et al.*, 2019). However, biocompatibility, improved magnetization, and active surface functionality are needed for the stability of the NPs

**Corresponding Author Email: gannadurai@msuniv.ac.in*

under a biological environment for biomedical applications (Gupta and Gupta, 2005). Fundamental parameters such as nanoparticle charge, solution stability, crystallization, zeta potential, nanoparticle coating, and synthetic methods would affect the biomedical applications (hyperthermia, drug delivery, transfections, cell tracking, tissue repair, and anti-tumor) (Vogel *et al.,* 2016). Multifunctional chitosan-coated iron oxide NPs possessing antimicrobial activity were applied as microbial resistance for biomedical instruments and the bilayer oleic acid-coated iron oxide NPs were found to get dissolved in inorganic solvents at ideal pH, which would contribute to the biomedical field (Ling *et al.,* 2019). The quality of iron oxide NPs depends on the crystallization, synthesis approaches, size, and shape so that the particle would be well-crystallized and size-controlled for better application (Ge *et al.,* 2009).

MATERIALS AND METHODS

All the chemicals were purchased from Hi-media (Mumbai). The following chemicals which are used in the experiments such as Ferric chloride ($FeCl_3$), Ferrous chloride ($FeCl_2$), Sodium hydroxide (NaOH), and Hydrochloric acid (HCl) were of analytical grade and used in its pure form without more purification.

Chemical Synthesis of Magnetic Nanoparticles: In a typical method, Sodium hydroxide (2 g) was dissolved in 50 ml of deionized water and stirred for half an hour using a magnetic stirrer. A solution of 5.2 g of $FeCl_3$ and 2 g of $FeCl_2$ was dissolved in 50 ml of deionized water. Burette solution of NaOH was allowed to be added to the Ferric and Ferrous chloride solution in a dropwise manner. The combined salt solutions were constantly stirred using a magnetic stirrer and the pH was measured. Black precipitates were formed due to the dropwise addition of NaOH solution. The whole reaction was continued for a further 30 min and the solution was allowed to settle for 1 h. After the solution was centrifuged at 6000 rpm using distilled water, the precipitate was washed with ethanol to remove the impurities. Furthermore, the sample was dried in a hot air oven at 60° C followed by annealing at 280° C for 2 h in a muffle furnace.

Antibacterial activity of IOMNPs: The antibacterial activity of chemically synthesized IOMNPs was assessed by Agar well diffusion method utilizing Muller-Hinton agar against pathogenic bacteria such as *Escherichia coli* (A), *Pseudomonas* (B), *Enterobacter* (C), *Staphylococcus aureus* (D), and *Bacillus subtilis* (E). Pathogenic bacteria are grown in nutrient broth. After 24 h of culture, these strains were swabbed uniformly onto the individual's plates containing Muller-Hinton agar using sterile cotton swabs. About 5 wells were made and the purified IOMNPs at different weights such as 0.1 mg and 0.5 mg were added into each well on all plates and *Streptomycin* was used as control. The plates were incubated for 24 h at 37°C in an incubator. After incubation, the different levels of zone formation around the well were measured.

RESULT AND DISCUSSION

XRD Analysis: X-ray diffraction (XRD) analysis is an effective characterization tool to confirm the crystal structure of the synthesized NPs. Fig 1. Shows the results of XRD analysis for the synthesized nanoparticles that were obtained with the concentrations of $FeCl_3$. The XRD pattern for IOMNPs showed diffraction peaks along (111), (012), (211), (220), (311), (422), and (217), respectively. The XRD pattern of IOMNPs shows three broad peaks at 2θ values 23°, 32°, and 53° that indicate its amorphous nature. The patterns have been compared with standard XRD for the Fe_2O_3 (hematite) (JCPDS data: PDF number 39-1346) (Balasubramanian, *et al.,* 2014). The average size of the NPs was calculated using the Debye-Scherer formula.

$$D = \frac{k}{\beta} Cos\ \theta \quad \text{D} = \text{k}\ \lambda/\beta\ \cos\theta$$

Where D is the particle size of the crystals, k is Scherer constant with the value from 0.9 to 1, β is the full width at the half-maximum value of XRD diffraction lines, λ is the X-ray wavelength and θ is the angle of Bragg's diffraction (Rahman *et al.,* 2017).

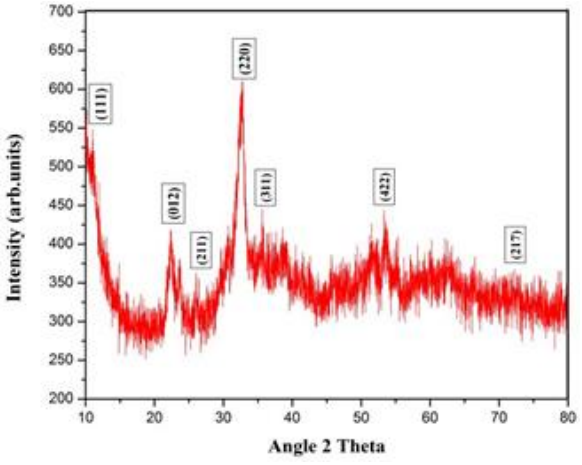

Fig 1: XRD analysis of synthesized IOMNPs

UV–vis spectroscopy: UV–Visible spectroscopy has been conducted to explore the optical properties of IOMNPs (Martin *et al.,* 2008). The reduction of Iron oxide magnetic nanoparticles (IOMNPs) was monitored by using a double beam UV-vis

spectrophotometer (Shimadzu, 96 UV-1900i model) (Bharathi *et al.,* 2020) of the reaction medium in the wavelength range of 280-900 nm with 1000 mm quartz cell. The resolution of the UV-vis spectrophotometer was 1 nm. The UV-vis spectrum of the resulting solution was recorded. The graph of wavelength on the X-axis and absorbance on the Y-axis was plotted. The optical properties of IOMNPs were monitored by using UV–Vis (Shimadzu, 96 UV-1900i model). The optical absorption coefficient has been calculated in the wavelength region of 280-900 nm. The absorption peak at 560 nm in Fig 2 confirmed the presence of IOMNPs (Mirza *et al.,* 2018) reported that UV-spectral absorbance between 250-260 has a unique characteristic feature of IOMNPs.

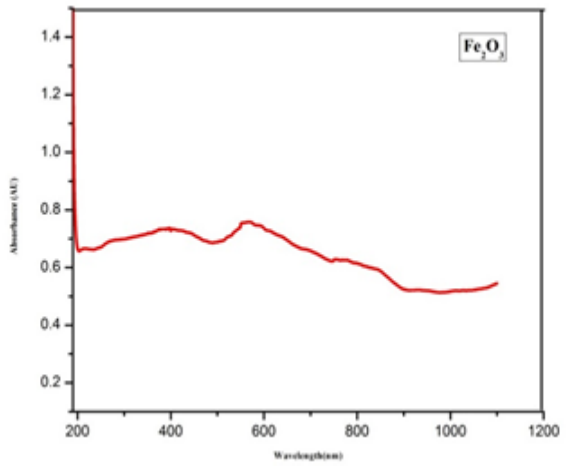

Fig 2: UV-Vis Spectrum of synthesized IOMNPs

SEM analysis: The Scanning Electron Microscopic analysis of Iron oxide NPs was done using Carl Zeiss Evo 18 Secondary Electron Microscope for better magnification up to 100K. The magnification depends on the sample size (Krishnaveni *et al.,* 2019). Morphology studies were done using SEM analysis of the synthesized IOMNPs as shown in Fig 3. The synthesized sample was dissolved in deionized water and maintained in a sonicator for 30 min. After the process was completed, one drop of the sonicated sample was placed on the silicon surface and finally dried on a hot plate. The obtained results using SEM analysis shown that IOMNPs has a spherical shape with little agglomeration. (Prodan *et al.,* 2013) have obtained the spherical shape while synthesizing IOMNPs in his studies.

FTIR analysis: The Fourier Transform Infra-Red Spectroscopy of IOMNPs was presented in Fig 4. The peak value and the corresponding functional groups are presented in Table 1. The peak arising at 3424 cm^{-1} is observed due to the O–H stretch of H–bonded alcohols, phenols. The -N=C=O stretch of isocyanates can be seen at 2270 cm^{-1}. The N–H bend of 1° amine can be found at 1644 cm^{-1}. The peaks at 1172 cm^{-1} attributes to the C–N stretch of aliphatic amines. N–O symmetric stretch of nitro compounds is observed around 682 cm^{-1}. The fingerprint region at 558 cm^{-1} shows the C–Br stretch of alkyl halides. The bands 586 is assigned to characteristic Fe–O vibrations of Fe_3O_4. The band O–H vibrations occur from 3160 to 3430 cm^{-1}. Slight differences occur in the peaks at 3414 cm^{-1} representing –OH functions. The band at 1616 cm^{-1} is due to the bending modes of the water molecules adsorbed on magnetite surfaces (Lopez *et al.,* 2010).

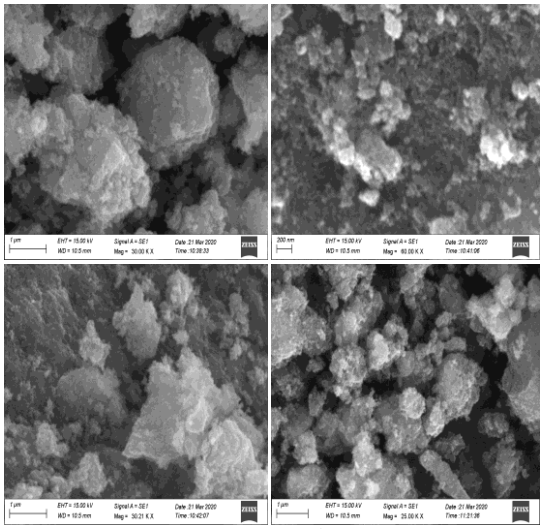

Fig 3: SEM Image of IOMNPs

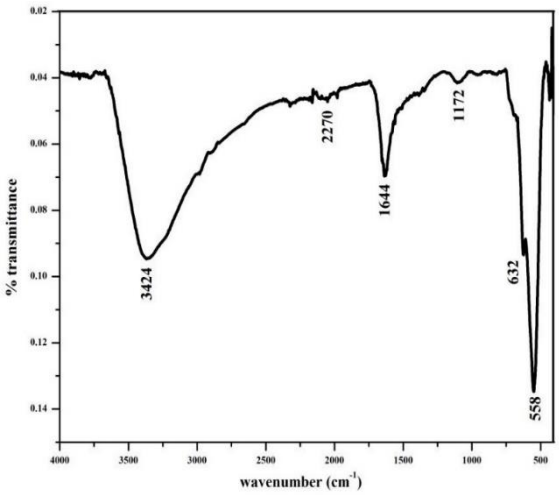

Fig 4: FTIR spectrum of IOMNPs

Table 1: Peak table of IOMNPs

S. No	Peak (cm^{-1})	Functional Group
1	3424	O–H stretch, H–bonded alcohols, phenols
2	2270	-N=C=O stretch isocyanates
3	1644	N–H bend 1° amines
4	1172	C–N stretch aliphatic amines
5	682	N–O symmetric stretch nitro compounds
6	558	C–Br stretch alkyl halides

DLS analysis: DLS is based on the laser diffraction method with multiple scattering techniques utilized to study the average particle size of sample nanoparticles. The synthesized sample was spread in deionized water followed by ultra-sonication. The solution was filtered out and centrifuged for 15 min at 25°C with 5000 rpm and the supernatant was collected. The supernatant was diluted 4-5 times and the particle distribution in the liquid was studied in a computer-controlled particle size analyzer (ZETA sizer Nano series, Malvern instrument Nano Zs) (Kaman and Dutta, 2018). The size distribution of the IOMNPs was measured by Dynamic Light Scattering (DLS). DLS uses a light source that emits through a solution containing particles and measures the amount of light reflected from the particles. The graph consists of size measurements concerning the intensity of scattered light, the volume of the sample, or the measured number of particles in the sample. The average particle size obtained in our study was 60 nm as shown in Fig 5.

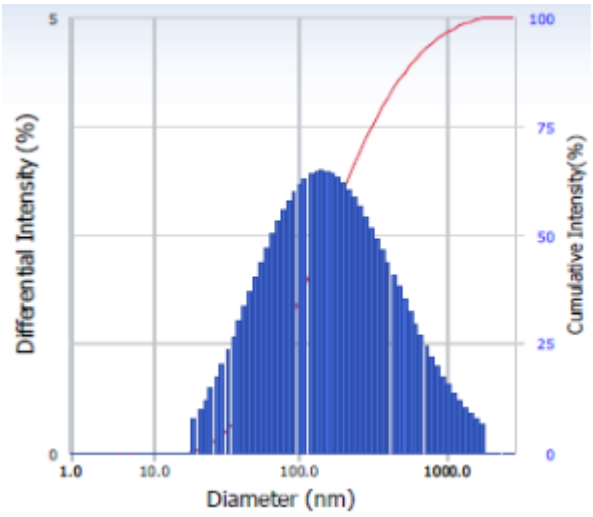

Fig 5: DLS Particle size image of IOMNPs

FL analysis: Fluorescence characterization of the IOMNPs was performed using an Instrument model LS45. The fluorescence measurements of Iron oxide NPs were also made over the wavelength range of 250-700 nm. The fluorescence spectrum of IOMNPs was recorded at room temperature by a Fluorescence spectrophotometer as shown in Fig. 6 Fluorescence spectrum is a useful technique for investigating energy levels. The lower emission peak at 383 nm was due to the radiating defects related to the interface traps existing at the grain boundaries. The higher emission at 680 nm may also attribute to the surface defects, and few authors reported that these peaks are related to the dislocations or oxygen defects. The fluorescence spectrum of IOMNPs present at a series of emissions in the region from 350 to 700 nm.

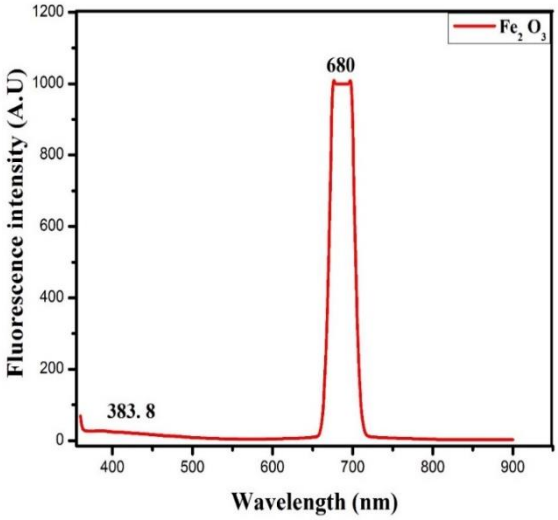

Fig 6: Fluorescence image of IOMNPs

TGA analysis: TGA is considered the most important method for studying the thermal stability of polymers and nanoparticles the thermal stability of the PANI-SnO2 Nanocomposite was investigated by using TG/DTA (Hitachi-Thermo Gravimetry/Differential Thermal Analyzer STA7000, Japan) analysis was performed from 30°C to 800°C with a heating rate of 10°C/min under nitrogen flow. The synthesized IOMNPs was analyzed by Thermogravimetric analysis for thermal sustainability and weight loss. TGA of dried iron oxide NPs at optimum concentration was observed after 24 h in air and was analyzed between the temperature of 20°C and 800°C in a nitrogen atmosphere at a heating rate of 20°C min^{-1}. The obtained curves are shown in Fig 7. The obtained results showed that two endothermic peaks were observed in the DTA curve under 80° C which attributed to desorption of water and CO physically adsorbed on the oxide surface with 1.9 mg weight loss on the TGA curve. An obvious exothermic peak appears between 120 and 420° C. This peak was related to maghemite to hematite phase transition without any weight loss on the TGA curve. The last endothermic peak at 460° C corresponded to the decomposition of hematite to wustite (FeO) attributed to the transition of hematite to magnetite with a 1.31 mg weight loss.

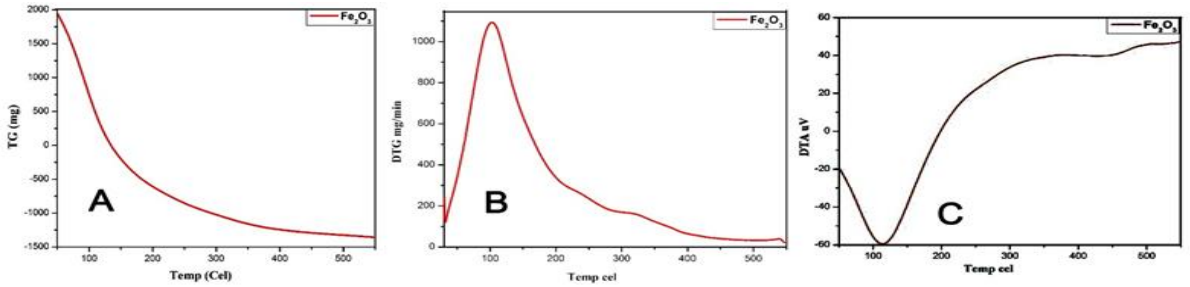

Fig 7: TG (A), DTG (B), and DTA (C) curves of IOMNPs

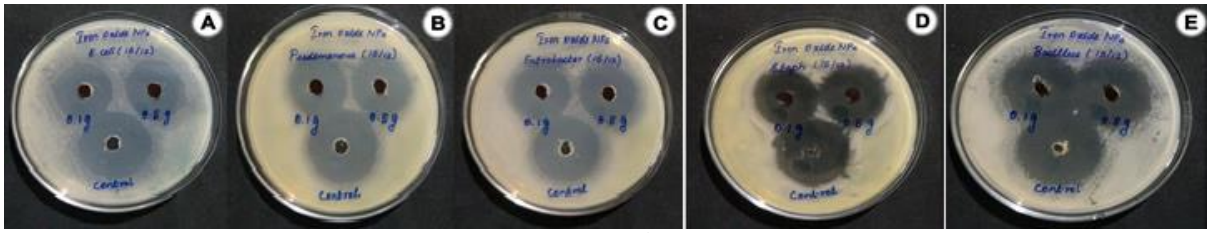

Fig 8: Antibacterial activities of synthesized IOMNPs

Table 2: Antibacterial activity of IOMNPs

Concentration	Zone of Inhibition (mm in diameter)				
	***E. coli* (A)**	***Pseudomonas* (B)**	***Enterobacter* (C)**	***Staphylococcus aureus* (D)**	***Bacillus* (E)**
0.1 mg	3	2.2	2.8	2.8	3
0.5 mg	3	2.4	2.8	3	3.2
Control	3.2	3.2	3.1	3.2	3.5

Antibacterial activity: The antibacterial activity of chemically synthesized IOMNPs was assessed against pathogenic bacteria such as *Escherichia coli* (A), *Pseudomonas* (B), *Enterobacter* (C), *Staphylococcus aureus* (D), and *Bacillus subtilis* (E) as shown in Fig 8. Table 2 showed that the antibacterial activity against *E. coli* and *Bacillus subtilis* was neutral at 0.1 mg concentration comparing the other bacterial species. The same result was obtained for *Enterobacter* and *Staphylococcus aureus.* At the concentration of 0.5 mg similar inhibition zone was observed between *E. coli* and *Staphylococcus aureus.* Higher antibacterial activity was observed in *Bacillus subtilis*, Gram-positive bacteria, and the lower antibacterial activity was observed in *Enterobacter*, Gram-negative bacteria. On altering the concentration, an increase in the antibacterial activity was observed in *Pseudomonas* (B), *Staphylococcus aureus* (D), and *Bacillus subtilis* (E) whereas *Escherichia coli* (A) and *Enterobacter* (C) shown similar inhibition zone.

Conclusion: The IOMNPs are synthesized, characterized, and assessed for antibacterial activity. The antibacterial activity for both Gram-positive and Gram-negative bacteria was performed with comparison in the concentration (0.1 and 0.5 mg). Higher antibacterial activity was observed in *Bacillus subtilis* (Gram-positive) and lower antibacterial activity was observed in *Pseudomonas* (Gram-negative). The applicability of IOMNPs was focused much on biomedical applications with the clinical trials conducted.

REFERENCES

Arsalani, S; Oliveira, J; Guidelli, EJ; Araujo, JFDF; Wiekhorst, F; Baffa, O (2020). Synthesis of radioluminescent iron oxide nanoparticles functionalized by anthracene for biomedical applications. *Colloids Surf, A Physicochem Eng Asp.* 602: 125105.

Balasubramanian, C; Joseph, B; Gupta, P; Saini, NL; Mukherjee, S; Di Gioacchino, D; Marcelli, A (2014). X-ray absorption spectroscopy characterization of iron-oxide nanoparticles synthesized by high temperature plasma processing. *J Electron Spectros Relat Phenomena*. 168: 125–129

Bharathi, D; Preethi, S; Abarna, K; Nithyasri, M; Kishore, P; Deepika, K (2020). Bio-inspired synthesis of flower shaped iron oxide nanoparticles (FeONPs) using phytochemicals of *Solanum lycopersicum* leaf extract for biomedical applications. *Biocatal. Agric. Biotechnol.* 27: 101698

Dadashi, S; Poursalehi, R; Delavari, H (2015).

Structural and Optical Properties of Pure Iron and Iron Oxide Nanoparticles Prepared via Pulsed Nd:YAG Laser Ablation in Liquid. *Procedia Materials Science*. 11: 722–726

Dadfar, SM; Roemhild, K; Drude, NI; Von Stillfried, S; Knüchel, R; Kiessling, F; Lammers, T (2019). Iron oxide nanoparticles: Diagnostic, therapeutic and theranostic applications. *Adv. Drug Deliv. Rev.* 138: 302–325

Estelrich, J; Escribano, E; Queralt, J; Busquets, M (2015). Iron Oxide Nanoparticles for Magnetically-Guided and Magnetically-Responsive Drug Delivery. *Int J Mol Sci*. 16(12): 8070–8101

Ge, S; Shi, X; Sun, K; Li, C; Uher, C; Baker, JR; Banaszak Holl, MM; Orr, BG (2009). Facile Hydrothermal Synthesis of Iron Oxide Nanoparticles with Tunable Magnetic Properties. *J. Phys. Chem. C*. 113(31): 13593–13599

Giustini, AJ; Petryk, AA; Cassim, SM; Tate, JA; Baker, I; HOOPES, PJ (2010). Magnetic Nanoparticle Hyperthermia in Cancer Treatment. *Nano LIFE*. *01*(01n02): 17–32

Gupta, AK; Gupta, M (2005). Synthesis and surface engineering of iron oxide nanoparticles for biomedical applications. *Biomaterials.* 26(18): 3995–4021

Kaman, PK; Dutta, P (2018). Synthesis, characterization and antifungal activity of biosynthesized silver nanoparticle. *Indian Phytopathology*. 72(1): 79–88

Krishnaveni, P; Priya, M; Annadurai, G (2019). Biosynthesis of Nanoceria from *Bacillus Subtilis*: Characterization and Antioxidant Potential. *Res. J. Life. Sci.* 5(3): 2454–6348

Ling, W; Wang, M; Xiong, C; Xie, D; Chen, Q; Chu, X; Qiu, X; Li, Y; Xiao, X (2019). Synthesis, surface modification, and applications of magnetic iron oxide nanoparticles. *J. Mater. Res.* 34(11): 1828–1844

Liu, D; Yang, F; Xiong, F; Gu, N (2016). The Smart Drug Delivery System and Its Clinical Potential. *Theranostics*, *6*(9), 1306–1323

Lopez, JA; González, F; Bonilla, FA; Zambrano, G; Gómez, ME (2010). Synthesis and characterization of Fe_3O_4 magnetic nanofluid. *Rev. Latinoam. de Metal. y Mater.* 30(1): 60–66

Martin, JE; Herzing, AA; Yan, W; Li, X; Koel, BE; Kiely, CJ; Zhang, W (2008). Determination of the Oxide Layer Thickness in Core−Shell Zerovalent Iron Nanoparticles. *Langmuir.* 24(8): 4329–4334

Mazrouaa, A; Mohamed, M; Fekry, M (2019). Physical and magnetic properties of iron oxide nanoparticles with a different molar ratio of ferrous and ferric. *Egypt. J. Pet.* 28(2): 165–171

Mirza, AU; Kareem, A; Nami, SAA; Khan, MS; Rehman, S; Bhat, SA; Mohammad, A; Nishat, N (2018). Biogenic synthesis of iron oxide nanoparticles using *Agrewia optiva* and *Prunus persica* phyto species: Characterization, antibacterial and antioxidant activity. *J. Photoch. Photobio B.* 185: 262–274

Nikolova, MP; Chavali, MS (2020). Metal Oxide Nanoparticles as Biomedical Materials. *Biomimetics*. *5*(2): 27

Prodan, AM; Iconaru, SL; Ciobanu, CS; Chifiriuc, MC; Stoicea, M; Predoi D (2013). Iron Oxide Magnetic Nanoparticles: Characterization and Toxicity Evaluation by In Vitro and In Vivo Assays. *J. Nanomater*.

Rahman, SSU; Qureshi, MT; Sultana, K; Rehman, W; Khan, MY; Asif, MH; Farooq, M; Sultana, N (2017). Single step growth of iron oxide nanoparticles and their use as glucose biosensor. *Results Phys*. 7: 4451–4456

Roy, R; Kumar, D; Sharma, A; Gupta, P; Chaudhari, BP; Tripathi, A; Das, M; Dwivedi, PD (2014). ZnO nanoparticles induced adjuvant effect via toll-like receptors and Src signaling in Balb/c mice. *Toxicol*. 230(3): 421–433

Shi, SF; Jia, JF; Guo, XK; Zhao, YP; Chen, DS; Guo, YY; Cheng, T; Zhang, XL (2012). Biocompatibility of chitosan-coated iron oxide nanoparticles with osteoblast cells. *Int. J. Nanomedicine*. 7: 5593–5602

Vogel, CFA; Charrier, JG; Wu, D; McFall, AS; Li, W; Abid, A; Kennedy, IM; Anastasio, C (2016). Physicochemical properties of iron oxide nanoparticles that contribute to cellular ROS-dependent signaling and acellular production of hydroxyl radical. *Free Radic. Res.* 50(11): 1153–1164